applied sciences

MDPI

Article

Rock Emissivity Measurement for Infrared Thermography Engineering Geological Applications

Simone Mineo * and Giovanna Pappalardo

Department of Biological, Geological and Environmental Sciences, University of Catania, 57, 95129 Catania, Italy; pappalar@unict.it

* Correspondence: smineo@unict.it

Featured Application: Quick and non-destructive applications of Infrared Thermography on rocks.

Abstract: Infrared thermography is a growing technology in the engineering geological field both for the remote survey of rock masses and as a laboratory tool for the non-destructive characterization of intact rock. In this latter case, its utility can be found either from a qualitative point of view, highlighting thermal contrasts on the rock surface, or from a quantitative point of view, involving the study of the surface temperature variations. Since the surface temperature of an object is proportional to its emissivity, the knowledge of this last value is crucial for the correct calibration of the instrument and for the achievement of reliable thermal outcomes. Although rock emissivity can be measured according to specific procedures, there is not always the time or possibility to carry out such measurements. Therefore, referring to reliable literature values is useful. In this frame, this paper aims at providing reference emissivity values belonging to 15 rock types among sedimentary, igneous and metamorphic categories, which underwent laboratory emissivity estimation by employing a high-sensitivity thermal camera. The results show that rocks can be defined as "emitters", with emissivity generally ranging from 0.89 to 0.99. Such variability arises from both their intrinsic properties, such as the presence of pores and the different thermal behavior of minerals, and the surface conditions, such as polishing treatments for ornamental stones. The resulting emissivity values are reported and commented on herein for each different studied lithology, thus providing not only a reference dataset for practical use, but also laying the foundation for further scientific studies, also aimed at widening the rock aspects to investigate through IRT.

Keywords: infrared thermography; rock; emissivity; laboratory test; surface temperature

Citation: Mineo, S.; Pappalardo, G. Rock Emissivity Measurement for Infrared Thermography Engineering Geological Applications. *Appl. Sci.* **2021**, *11*, 3773. https://doi.org/10.3390/app11093773

Academic Editors: Birendra Jha and Giovanni Maria Carlomagno

Received: 25 March 2021
Accepted: 19 April 2021
Published: 22 April 2021

1. Introduction

Infrared thermography (IRT) is a scientific application for the acquisition and analysis of thermal information, based on the detection of the thermal radiation emitted by an object. At temperatures above absolute zero, all bodies emit electromagnetic radiation, with wavelengths mainly falling within the infrared band of the electromagnetic spectrum, as the result of thermally excited electron oscillations or transitions within the matter [1,2]. Infrared radiation is therefore invisible to the human eye and specific devices are required to process such signals. These are infrared cameras, which can detect and record the radiation emitted by a material to build a thermal image, from which the temperature pattern can be reconstructed. The feature controlling the relation between the emitted radiation and the surface temperature of the investigated material is known as emissivity (ε) [3]. This surface property, characterizing all forms of matter capable of emitting thermal radiation, ranges between 0 (referred to as a perfect emitter—mirror) and 1 (referred to as a theoretical perfect absorber—blackbody). Based on this value, the surface temperature of an object can be quickly estimated in a non-destructive way. Thanks to this, IRT has experienced a growing diffusion across a wide range of scientific fields; a literature review [4] and

references therein highlighted that IRT is employed in medicine or biology, chemistry, engineering and material science, life and sport sciences, meteorology and agriculture, although the most predominant fields involving IRT applications are applied science and engineering. In the latter cases, the use of IRT is also focused on building materials and structures characterization: Al-Hadhrami et al. [5] studied the thermal behavior of concrete specimens aiming at assessing their density, while Huh et al. [6] and Janku et al. [7] employed IRT to detect deterioration signals in concrete structures. More recently, IRT has found its utility even in engineering geological sciences, with satisfactory results in the study of landslides, hydrogeology and rock mechanics, e.g., [8–14]. With specific reference to rock materials, Mineo and Pappalardo [15] used IRT for the indirect estimation of rock porosity in laboratory, while Huang at al. [16] and Danov et al. [17] suggest that rock spectral emissivity is subject to variation during mechanical loading and with respect to the rock composition, respectively. Estimating the emissivity of a rock is possible according to specific procedures, although often, it is useful to have a reference value due to time issues or the impossibility of measuring. NASA's ECOSTRESS (ECOsystem Spaceborne Thermal Radiometer Experiment on Space Station) Spectral library [18,19] is a good reference in terms of the reflectance spectra of rocks, minerals, lunar/terrestrial soils covering the visible through thermal infrared wavelength region (0.4–15.4 μm). FLIR Systems [20] collected several experimental data on emissivity values belonging to different materials. The provided table, compiled by using a shortwave camera (i.e., a camera sensitive to shorter IR wavelengths between visible light and 3 μm), lists numerous kinds of material, but only a few examples of rocks. Some articles provide a mention on the emissivity of marble, granite, sandstone, limestone and gypsum, due to their employment in constructions, clay and soil [21,22]. On this trend, this paper aims at increasing the scientific casuistry providing representative emissivity values for different rock types, according to their laboratory assessment through the method suggested by FLIR [20]. Specimens of igneous, sedimentary and metamorphic rocks were chosen among the most common lithologies considered for engineering geological and cultural heritage purposes. The applied laboratory procedure allowed the estimation of a range of suitable emissivity values for 15 different rock types, which are herein made available to the scientific community and commented on, shedding light on new potential IRT applications.

2. IRT Background

Infrared radiation, or infrared light, is part of the electromagnetic spectrum (Figure 1). Due to its wavelength (700–1 mm) the human eye cannot see it, but humans can sense some of this energy as heat [23]. According to the temperature of an object, most of its infrared radiation can be "seen" by specific devices known as thermal cameras, which convert infrared radiation into visible images [24]. According to the Wien's displacement law, the peak wavelength of the emitted radiation is inversely proportional to the temperature. For a body at ambient temperature, the peak occurs in the infrared band (Figure 1). For this reason, thermal imaging is considered a very powerful remote sensing technique for numerous field studies, thanks to the fact that thermal radiation can penetrate smokes, aerosols, dust, and mists more effectively than visible radiation [24].

The Stefan–Boltzmann law (Equation (1)), explains the relationship between the energy emitted by a body (J), across all wavelengths, and the Stefan–Boltzmann constant (σ), the surface temperature of the body (T) to the fourth power and its emissivity (ε) [25]:

$$J = \varepsilon \sigma T^4 \quad (1)$$

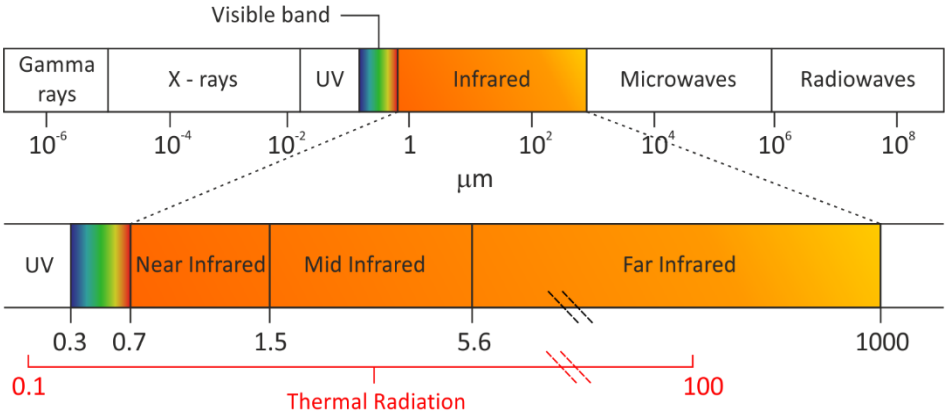

Figure 1. The electromagnetic spectrum with the range of occurrence of thermal radiation and the infrared band highlighted.

Mathematically, emissivity is the ratio between the infrared radiation emitted by a body and the radiation emitted by a blackbody at the same temperature. It is self-evident that it plays an essential role in infrared thermographic surveys and it is dependent on temperature, wavelength and surface condition [3]. For example, a surface with a low emissivity value (i.e., aluminum, steel, etc.) acts as a mirror (high reflectance).

With reference to the engineering geology, IRT use represents a new frontier for both the remote surveys of landslides/rock masses and rock mechanics laboratory applications. It has proved a useful tool in detecting crevasses, cave openings and rock fracturing [26–28], or the integrity of rock mass behind a shotcreted slope [14]. Some authors [29] tested the application of IRT to rock masses under different daily and seasonal conditions, finding out a statistical relation between the rock mass cooling and its grade of fracturing. Based on such innovative results, Pappalardo et al. [30] used IRT to characterize unstable rock wedges, while Fiorucci et al. [31] studied the thermal response of jointed rock masses. IRT was further employed to characterize landslides, even in combination with other remote survey or geophysical techniques, e.g., [32–34], and for the detection of rock bridges within rock mass cracks [35]. Further applications refer to the study of rock behavior under stress, where IRT can highlight the unstable crack propagation and/or flaw coalescence [36], to the evolution monitoring of excavation damaged zones [37], and to the detection of microstructural changes of reservoir rocks [38].

A parallel pioneering scientific trend is the indirect estimation of rock porosity in laboratory by using IRT to monitor the cooling rate of oven-heated rock specimens. More specifically, the strong relationship existing between the rock porosity and its cooling speed has recently been highlighted, demonstrating that a porous rock cools faster than a massive one [15,39]. Such evidence leads the way to a potentially increasing number of IRT applications on rocks, which must be supported by reliable data. In this light, the emissivity knowledge of a framed target is essential to achieve a correct estimation of its surface temperature by IRT. For this reason, emissivity values belonging to different natural and human-made matters have been experimentally estimated and are available in the literature, although there are few data on rocks [20]. Among the low-emissivity materials, polished bronze, copper, chromium, iron, steel, gold and platinum can be found, while masonry bricks, asphalt pavement, concrete, carbon and human skin are counted among the high-emissivity materials. With reference to rock applications, available and quickly usable values belong to rocks employed for decorative and construction purposes, such as fired clay (ε = 0.91), granite (ε = 0.77–0.97), gypsum (ε = 0.8–0.9), sand (ε = 0.6–0.9), sandstone (ε = 0.909–0.935), and soil (ε = 0.92–0.95 in dry and saturated condition, respectively) [20], thus highlighting the need of implementing such scientific casuistry, which is the aim of this paper.

3. Materials

The targets of this research are 27 specimens belonging to 15 different rock types chosen among sedimentary, igneous and metamorphic categories (Figure 2). Specimens offer a planar surface, either smooth or polished, to be framed by IRT.

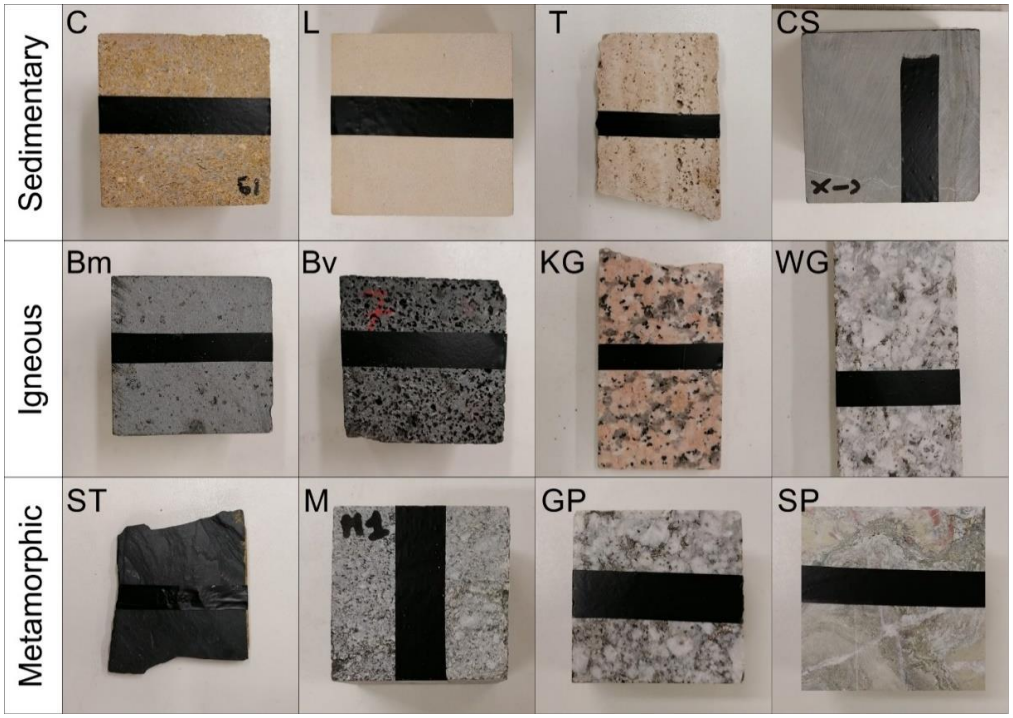

Figure 2. Some representative specimens belonging to the different rock categories tested herein.

The sedimentary lithologies taken into account herein include:

- Limestones (L): fine-grained, light beige, limestone with a porous texture, showing millimetric voids and rare traces of bioturbation. This rock type was specifically employed for the reconstruction of a UNESCO world heritage monument in south-eastern Sicily.
- Calcarenites (C): two varieties of sicilian calcarenites were tested herein. The first is known as Sabucina stone, classifiable as a yellowish biosparite, with allochems mainly given by small fragments of foraminifera/bryozoa and orthochems represented by spathic calcite and small amount of micrite [39] and reference therein. The second belongs to the "Panchina" formation and it is a yellowish organogen calcarenite. Rocks show a porous texture, with micro and macro voids up to millimetric size.
- Quartzarenites (QA): belonging to the arenaceous member of a Flysch succession, such greyish rocks contain sharp to sub-rounded lithic fragments (<1 mm) and widely crop out in northeastern Sicily.
- Calcisiltite (CS): dark grey marly calcisiltites, with rare mineral clasts in a microcrystalline carbonate cement.
- Sandstones (S): yellowish to grayish sandstones affected by a grain-size variability, from fine-to medium belonging to the Capo d'Orlando Flysch formation of northern Sicily. Such sandstones have been defined as quartzofeldspathic arcoses [40] and references therein.
- Dolostones (D): cropping out on the Peloritani Mountains (northeastern Sicily) and belonging to the Longi-Taormina Unit, these rocks are characterized by a massive to brecciated structure and show the occurrence of calcite veins. Color ranges from grey to a light pink.

- Travertine (T): cream-colored banded rock composed of calcite, usually formed by the evaporation of river and precipitation of carbonate minerals at spring waters. It is a variety of rock often used for walls and interior decorations.

Igneous samples are:

- Basalt: volcanic, effusive rocks from Mount Etna. At hand-scale, specimens show a porphyritic texture with a massive (Bm) or vesicular (Bv) structure. In the first case, olivine, pyroxene and plagioclase crystals are found in a groundmass and no visible voids can be detected; in the second case, millimetric voids occur within the rock structure, e.g., [41].
- Granite: coarse-grained igneous rock mainly composed of quartz, alkali feldspar, and plagioclase tested herein in three different varieties, i.e., alkali feldspar granite also known as "red granite" with both polished (AGp) and smooth (AGs) surface; K-feldspar pinkish granite with both polished (KGp) and smooth (KGs) surface; white plagioclase granite (WG) with a smooth surface.
- Tuff (TF): medium grain sized volcanic grayish rock, with plagioclase, biotite, with pumice concentration.

Metamorphic samples are:

- Migmatites (M): massive and fracture-free rocks, with the occurrence of banding given by millimetric alternation of leucocratic and melanocratic portions. The mineral content is represented by quartz, plagioclase, biotite and muscovite with minor chlorite, K-feldspar, and sillimanite.
- Serpentinites (SP): dark green rocks sometimes affected by affected by serpentine and calcite veins.
- Slate (ST): black fine-grained, foliated, low-grade metamorphic rock derived from an original shale-type sedimentary rock composed of clay or volcanic ash.
- Granitoid plutonites (GP): holocrystalline rocks with a faneritic texture mainly composed of quartz, plagioclase, biotite and muscovite.
- Marble: white metamorphic rock composed of recrystallized carbonate minerals from a limestone or dolomite protolith, with both polished (MBp) and smooth (MBs) surface.

4. Methodology

The experimental methodology for the emissivity estimation was carried out herein according to [20,42] by employing a high-sensitivity thermal camera FLIR T420 (Table 1). It is a non-contact measurement method requiring the use of an emissivity-known surface material. In this case, a piece of electrical tape, with known high emissivity (ε = 0.97), was placed on the specimen face, adjacent to the area where the emissivity was to be measured (Figure 3). This method is based on the rock emissivity estimation by comparing its optic features with the ones of a nearby blackbody at the same temperature, simulated by the black tape [43]. The rock was then oven-heated to reach, at least, 20 K above room temperature, according to the specifications, and the temperature difference between the specimen and the ambient was stable during the quick test, thus minimizing potential measurement errors.

Table 1. Main technical specification of the employed thermal camera.

IR resolution	320 × 240 pixels
Object temperature range	−20 °C to +120 °C (−4 °F to +248 °F) 0 °C to +650 °C (+32 °F to +1202 °F)
Accuracy	±2 °C (±3.6 °F)
Spectral range	7.5–13 μm
Focal Plane Array	Uncooled microbolometer

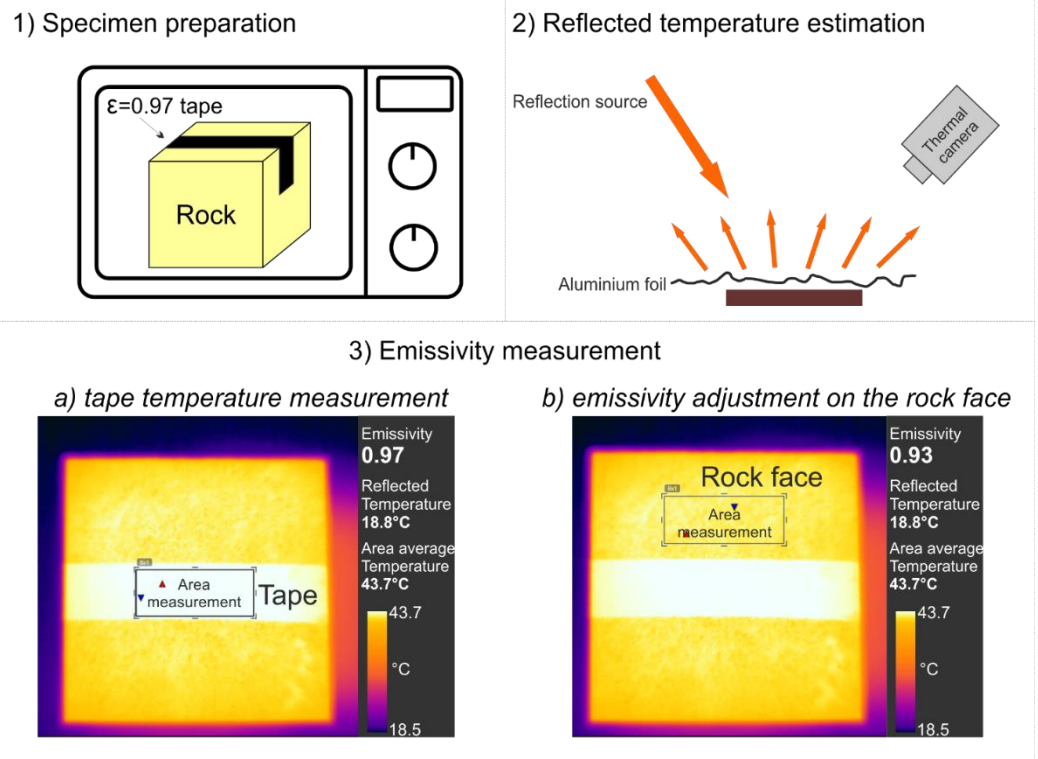

Figure 3. Phases of the methodological approach carried out to determine the emissivity of rock specimens. Sketch in inset (2) is modified from [20].

The second step (Figure 3) was the determination of reflected apparent temperature, i.e., a parameter used to compensate the radiation reflected in the object [44]. This step is crucial, because it allows the avoidance of potential error sources. The reflected apparent temperature was estimated herein according to the "reflector method", which consists in crumbling up a large piece of aluminum foil and then unscrambling it on a piece of cardboard of the same size. This was placed in front of the target to frame and pointed by the thermal camera with the emissivity set to 1.0. The apparent temperature of the aluminum foil was measured. Since laboratory measurements were carried out from an acquisition distance of 0.4 m, atmosphere effects were negligible. Moreover, the experimental set was a laboratory room with constant ambient temperature and humidity and no artificial sources of light; heating conditions were constant for all the specimens, so this ensured a strong reduction in potential measuring errors.

For the emissivity determination, the rock specimen with the attached electrical tape was placed in front of the camera, after having verified that the tape was in good contact with the specimen, and the IRT image was taken. Such an image was processed by the software Flir Tools, which allowed one to adjust the level and span for best image brightness and contrast. Emissivity was set according to the tape value and the reflected temperature was set according to the previous measure. The temperature of the tape (Tt) was measured according to the "area function" (indicated for surfaces with varying emissivity such as rocks composed of different minerals or affected by voids). Then, the measurement function was moved to the sample surface and the emissivity setting was adjusted until the same temperature Tt was recorded. The emissivity corresponding at the Tt detected on the rock surface was the emissivity of the tested rock.

Furthermore, measures were repeated a minimum of three times and at different portions of the specimen surface. This was carried out because the rock surface may be affected by specific macroscopic features, such as a preponderant concentration of pores or minerals, which could play a role on the final emissivity value. Therefore, in order to find out their influence on emissivity, along with a reliable range of values to be considered

representative of the entire framed surface, measuring area tools were located at different portions of the rock face and emissivity was measured at different rock face sectors. The results were then compared to find out the average emissivity value to be considered representative for the tested rock types. Considerations on the main controlling features are provided.

5. Results

The values estimated herein fall within a general 0.83–0.99 emissivity range (Figure 4a), with the sedimentary rock group affected by the narrowest interval ($0.91 < \varepsilon < 0.99$), followed by the metamorphic ($0.89 < \varepsilon < 0.99$) and igneous ($0.83 < \varepsilon < 0.98$) categories (Figure 4b). The width of this last case arises from the lowest ε estimated on two polished granite samples, without which the emissivity igneous range would have overlapped with the others (rock $\varepsilon \geq 0.89$). The resulting values for each rock type are listed in Table 2 in alphabetic order.

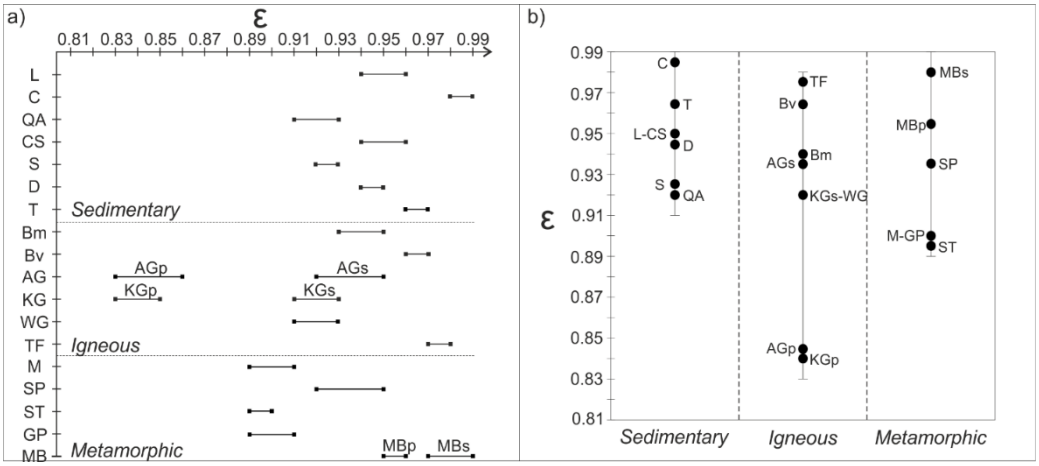

Figure 4. (**a**) Emissivity ranges resulting for each tested rock type; (**b**) statistical plot of the emissivity ranges for the three sedimentary, igneous, and metamorphic rock groups. Whiskers represent maximum and minimum values, while dots indicate the average emissivity for each rock type (acronyms are listed in Table 2).

5.1. Sedimentary Rocks

The lowest ε values are related to quartzarenites and sandstones, both showing a coarse-grained structure and the presence of quartz minerals. The sandstone average ε (0.935) matches with the literature's available data for the same rock type provided by FLIR [20]. The intermediate sedimentary average ε values (0.945–0.95) belong to dolostone, limestone and calcisiltite, united by the carbonate rock nature and the fine-grained structure with a variable micro-porosity. The greatest values refer to travertine and calcarenite samples, which are also carbonate rocks, although they are formed by different processes, but affected by macroscopic porosity. In fact, both rock types are characterized by a surface hosting millimetric to centimetric visible voids with different persistence (Figure 2).

5.2. Igneous Rocks

Igneous rock samples can be divided herein into two sub-groups: polished and smooth. The polished variety results from rock manufacturing processes aimed at their ornamental use, while smooth faces are proper of the natural aspect of rocks undergoing laboratory tests. Starting from the lower part of the range, polished granites are characterized by $0.83 < \varepsilon < 0.86$, with no relevant distinction between the slightly different mineral composition and color of tested rocks. This result is in accordance with the available literature data on the same polished rock type, reporting an average emissivity of 0.849 [20]. Smooth light granite samples are characterized by an average 0.92 emissivity, while the darker variety

(red granite) shows a wider range, partially overlapping with the previous one (Figure 4a), with a 0.935 mean value. Basalt rocks rank above the holocrystalline samples, with a mean ε= 0.94 for the massive variety and 0.965 for the vesicular one, followed by the highest tuff value (mean ε = 0.975).

Table 2. Emissivity values estimated for the tested rock types.

Rock Type	Acronym	Emissivity Range	Average Emissivity
Basalt (massive)	Bm	0.93–0.95	0.94
Basalt (vesicular)	Bv	0.96–0.97	0.965
Calcarenite	C	0.98–0.99	0.985
Calcisiltite	CS	0.94–0.96	0.95
Dolostone	D	0.94–0.95	0.945
Granite (polished)	WGp-KGp	0.83–0.85	0.84
Granite (smooth)	WGs-KGs	0.91–0.93	0.92
Granitoid plutonite	GP	0.89–0.91	0.90
Limestone	L	0.94–0.96	0.95
Marble (polished)	MBp	0.95–0.96	0.956
Marble (smooth)	MBs	0.97–0.99	0.98
Migmatite	M	0.89–0.91	0.90
Quartzarenite	QA	0.91–0.93	0.92
Red granite (smooth)	AKs	0.92–0.95	0.935
Red granite (polished)	AKp	0.83–0.86	0.845
Sandstone	S	0.92–0.93	0.925
Serpentinite	SP	0.92–0.95	0.935
Slate	ST	0.89–0.90	0.895
Travertine	T	0.96–0.97	0.965
Tuff	TF	0.97–0.98	0.975

5.3. Metamorphic Rocks

With reference to the metamorphic group, slates hold the lowest emissivity (mean 0.895), followed by migmatites and granitoids, which are two macroscopically similar rock types (Figure 4). Serpentinite is characterized by a wider emissivity range (0.92–0.95), due to mineralogical heterogeneity of its surface. At the ranking top, marble samples are found, with an emissivity difference based on the polished or smooth surface condition. As for igneous granites, the polished marble sample is characterized by a lower ε (0.955 against 0.98 belonging to the smooth one).

6. Discussion

The achieved results pave the way to multiple discussion points, starting from the fact that a univocal emissivity value for each rock type could not be detected, but rather a range of values (Figure 4a). This is likely due to the effect of some features, which lead to an uneven thermal behavior of the framed rock surface. In fact, by moving the measuring area during the image processing, slight temperature and emissivity variations were experienced (Figure 5a). This suggests the need to define a representative ε value for IRT applications on rocks, whose approach is focused on the framing of the whole rock specimen surface, rather than on a small portion (e.g., voids or crystals). Therefore, it is reasonable to consider the mean value of the ranges found herein for each rock type as the representative emissivity. This choice is quite objective, also thanks to the narrow ε range extension of each rock type, which generally involves two or maximum three consecutive values (Figure 4a).

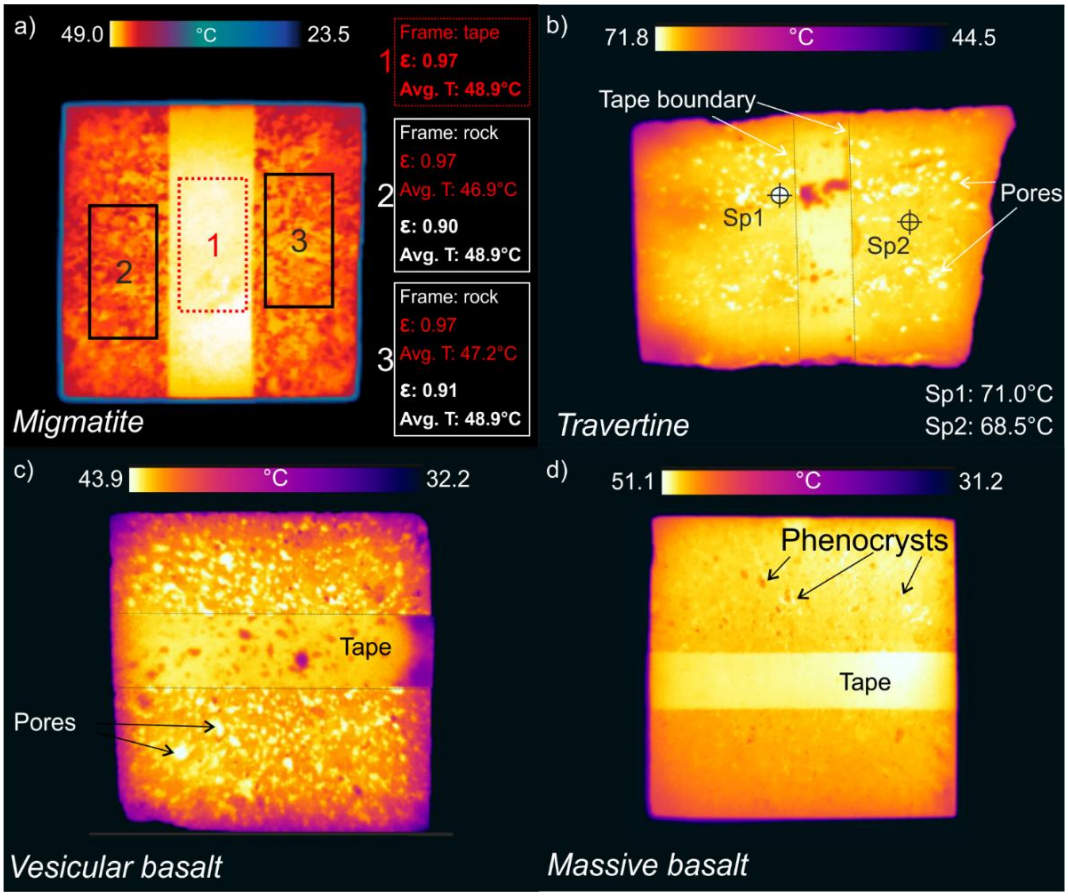

Figure 5. (**a**) Explanatory sketch for the slight emissivity differences occurring within the rocks: a specimen of migmatite characterized by a characteristic emissivity ranging between 0.90 and 0.91; (**b**) pore effect on the surface temperature variation of a travertine sample; (**c**) example of vesicular basalt with voids highlighted by the highest surface temperatures; (**d**) example of massive basalt where no voids affect the specimen surface. In this case, phenocrysts are highlighted by temperature contrast with the groundmass.

Based on the above consideration, a discussion on the effects causing such slight emissivity variations deserves to be proposed. According to achieved results, two main macroscopic features can be, indeed, indicated as "emissivity controllers", i.e., the presence of pores and mineral composition.

6.1. Pore Effect

In the frame of the relationship between rock porosity and IRT, it was demonstrated that the presence of macroscopic voids on a framed rock causes surface temperature variations [45]. In particular, macropores occurring within an oven-heated rock sample are labeled by a higher surface temperature than the rock matrix, with the greatest values recurring at the most persistent voids. This suggests that the IRT output of a rock surface is controlled by the presence of voids (Figure 5b). Such an effect, from now on referred to as the "pore effect", was detected herein; for example, at the carbonate rock group, where the massive or microporous dolostone, limestone and calcisiltite keep a lower emissivity than the macroporous travertine and calcarenite samples (Figure 4a). It must be underlined that this discussion point only involves the presence of macroscopic porosity, whose surface temperature can be detected by an infrared camera, regardless of the porosity percentage of the rock. A similar outcome can be highlighted for basalts, in their massive ($\varepsilon = 0.94$) and vesicular ($\varepsilon = 0.965$) varieties (Figure 5c,d). Even in this case, samples affected by macropores returned a higher emissivity due to the higher surface temperature of vesicles. Once it is further proved that the presence of voids affects the surface temperature

distribution on the rock surface and considering that voids can be represented both by pores and by cracks, a reasonable hint for future studies could be represented by the tentative correlation between the emissivity dispersion and the presence of cracks/damage zones within the rock itself.

6.2. Mineral Effect

Rock surface temperature variation is not controlled only by pores, but also by the macroscopically occurring mineral phases. The "mineral effect" can be well observed in thermograms belonging to holocrystalline rocks, where crystals can be distinguished according to their different surface temperature. In granite, for example, micas are characterized by the highest surface temperature (approximate estimated ε = 0.97–0.98), while feldspars own intermediate values (approximate estimated ε = 0.85–0.89) and quartz is the coldest phase (approximate estimated ε = 0.77–0.80) (Figure 6a,b). This proves the heterogeneity of such rock types with respect to emissivity, supporting the need of weighting the representative rock emissivity value on the whole framed surface. This outcome paves the way for further studies aimed at shedding light on a new potential IRT application as a tentative mineral mapping tool for crystalline rocks.

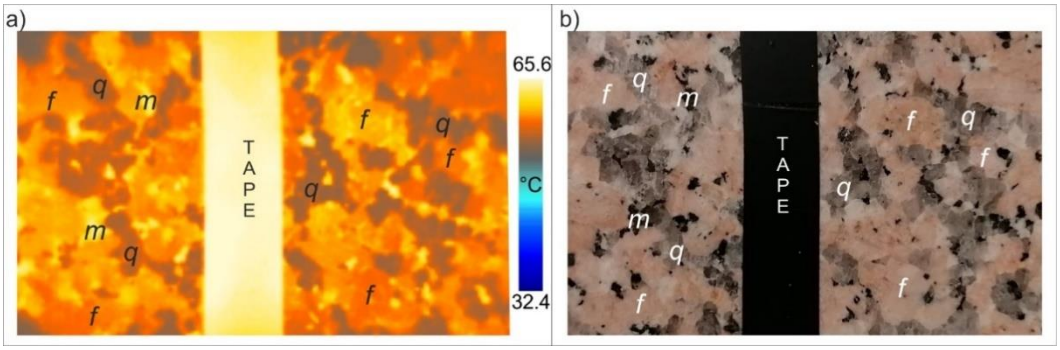

Figure 6. (**a**) IRT image of a granite highlighting the different thermal behavior offered by minerals, m—micas, f—feldspars, q—quartz; (**b**) digital image of the corresponding granite.

A kind of mineral effect can be also hypothesized for sedimentary rocks, although no visible crystals occur, where the quartz content of quartzarenite and sandstone could be responsible for their lower emissivity if compared to limestone and calcisiltite of the same rock group.

6.3. Consideration on a Possible Color Effect

The mineral effect observed at granites and migmatites may suggest a sort of color-dependance of emissivity. In fact, it has been experienced herein that higher ε values correspond to darker minerals (micas). This would also justify the higher mean emissivity of red granites (darker variety) if compared to the lighter ones (Figure 4a).

Nevertheless, single mineral phases are not the target of IRT for engineering geological applications, which is instead focused on framing the whole rock surface, on which both pore and mineral effects take place. In this perspective, a color-emissivity dependance was not found herein, as dark colored rocks are not always characterized by the highest emissivity values. An example is the case of light beige limestone vs. dark grey calcisiltite, which returned the same emissivity although showing an evident color difference to the naked eye; similarly, black slate holds a lower ε than white marble (Figures 2–4). This is not surprising; in fact, colors surely affect the visible light wavelength, which has the highest energy in the electromagnetic spectrum according to Planck's law, but at the infrared eye, only slight differences occur. Rather, such discrepancies can be explained by a mix of simultaneous mineral and pore effects, although differently weighted on the framed rock surface. In fact, the mineral effect plays a preponderant role on the emissivity of

macroscopically holocrystalline rocks, where crystals dominate the framed area. Similarly, in the case of light beige limestone vs. dark grey calcisiltite, the carbonate nature is common to both rocks, as well as the absence of macropores. On the contrary, the emissivity of a rock affected by the presence of voids is strongly influenced by the pore effect, which overcomes the eventual mineralogical differences.

These considerations further confirm the reasonability of choosing an average emissivity value for IRT applications on rocks when the framing of an "averaged" rock surface is required.

6.4. Rock Surface Manufacturing

A final discussion point is focused on the differences arising from the rock surface condition in case of ornamental stones, such as the granites and marble tested herein in the polished and smooth versions. Observed results show that polished varieties are affected by lower emissivity than the corresponding smooth ones. This is due to the different reflection power gained by polished surfaces, which act more as reflectors (mirrors), thus are characterized by a lower emissivity [20]. Therefore, the choice of a proper emissivity value prior to the thermal image processing is needed, especially if quantitative considerations have to be carried out. This represents a key point considering the growing application of IRT to cultural heritage and ornamental stones.

7. Conclusions

In this paper, the experimental estimation of rock emissivity was carried out to provide new scientific data on the use of infrared thermography (IRT) for engineering geological purposes. The development of new survey remote methodologies has opened the way to the application of IRT in laboratory and field activities involving rocks, through both qualitative and quantitative approaches. In the second case, the surface temperature of a rock framed by a thermal camera can be properly estimated by knowing its characteristic emissivity. In this paper, the emissivity was estimated herein on 27 oven-heated specimens belonging to 15 different lithologies among sedimentary, igneous and metamorphic ones by employing a thermal camera operating in the 7.5–13 μm spectral range. The achieved results show that tested rocks are characterized by high emissivity values, generally greater than 0.89, with the exception of polished rock granite surfaces, which show a slightly lower value due to the reflection effect brought by the polishing treatment (Figure 7). Moreover, each rock type is not characterized by a univocal emissivity value, but rather by narrow ranges of variability arising from the heterogeneity of the rock surface. In fact, it must be taken into account that rocks are natural aggregates of mineral affected by different textural features playing a key role on their emissivity. The first effect observed herein is played by pores, whose presence leads to the basic physical property known as porosity. In this case, the key controlling element is the presence of macroscopic pores, whose IRT attitude in oven-heated specimens is a high surface temperature at the pore location. Therefore, it is self-evident that the emissivity of a rock surface is conditioned by pores, which contribute to enhance its value (Figure 7). A further controlling feature is the mineralogical content, which is particularly evident for holocrystalline rocks, where minerals are macroscopically recognizable according to their different thermal behavior. It was experienced herein that the IRT output of dark minerals, such as micas in granites, is represented by positive anomalies (high temperatures) and high emissivity, while lighter minerals, such as quartz, are affected by lower temperature and emissivity (Figure 7). Therefore, both pore and mineral effects play a controlling role on the rock emissivity, although with different weights depending upon the rock type (the emissivity of holocrystalline rocks with no macroscopic pores is more affected by the mineral effect, while sedimentary porous rocks mainly respond to the pore effect). The combination of such two effects is so relevant that the rock color, at the hand scale specimen, seems not to produce relevant emissivity variations. Based on such considerations and for IRT applications requiring a general framing of the rock surface, it is reasonable to overcome these effects by considering an

average emissivity value for each rock type. Nevertheless, cases of same rock types but with different porosity must be distinguished (e.g., massive and vesicular basalts).

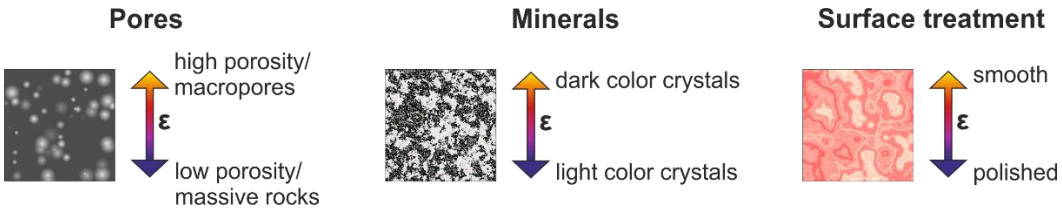

Figure 7. Graphical summary of achieved results with reference to the effects played on rock emissivity by pores, minerals and surface condition.

The results achieved herein surely represent a scientific step forward in the employment of IRT to rocks and pave the way to further studies aiming not only at increasing the scientific casuistry, but also at shedding light on new potential use of the IRT technology on rocks.

Author Contributions: Conceptualization, S.M.; methodology, S.M. and G.P.; software, S.M.; validation, S.M. and G.P.; formal analysis, S.M.; investigation, S.M.; data curation, S.M.; writing—review and editing, S.M.; visualization, G.P.; supervision, S.M. and G.P.; project administration, G.P.; funding acquisition, G.P. All authors have read and agreed to the published version of the manuscript.

Funding: This paper was financially supported by the Department of Biological, Geological and Environmental Sciences, University of Catania, Project: "CH2V—Cultural Heritage Hazard and Vulnerability", granted to Giovanna Pappalardo.

Acknowledgments: Emissivity estimation was carried out at the "Geologia Applicata" laboratory of the Department of Geological, Biological and Environmental Sciences of Catania University. The authors thank LAND (Laboratorio Analisi Non Distruttive) of the same department for lending the thermal camera.

Conflicts of Interest: The authors declare no conflict of interest.

References

1. DeWitt, N. *Theory and Practice of Radiation Thermometry*; Wiley: New York, NY, USA, 1988.
2. Wolfe, W.L.; Zissis, G.J. *The Infrared Handbook*; Office of Naval Research: Washington, DC, USA, 1993.
3. Avdelidis, N.P.; Gan, T.-H.; Ibarra-Castanedo, C.; Maldague, X.P.V. Infrared Thermography as a Non-Destructive Tool for Materials Characterisation and Assessment Paper. In Proceedings of the Thermosense: Thermal Infrared Applications XXXIII 2011, Orlando, FL, USA, 26–28 April 2011.
4. Ammer, K. Thermography 2015—A computer-assisted literature survey. *Thermol. Int.* **2016**, *26*, 5–42.
5. Al-Hadhrami, L.M.; Maslehuddin, M.; Shameem, M.; Ali, M.R. Assessing concrete density using infrared thermographic (IRT) images. *Infrared Phys. Technol.* **2012**, *55*, 442–448. [CrossRef]
6. Huh, J.; Tran, Q.H.; Lee, J.-H.; Han, D.; Ahn, J.-H.; Yim, S. Experimental Study on Detection of Deterioration in Concrete Using Infrared Thermography Technique. *Adv. Mater. Sci. Eng.* **2016**. [CrossRef]
7. Janku, M.; Brezina, I.; Grosek, J. Use of Infrared Thermography to detect defects on concrete bridges. *Procedia Eng.* **2017**, *190*, 62–69. [CrossRef]
8. Barla, G.; Antolini, F.; Gigli, G. 3D Laser scanner and thermography for tunnel discontinuity mapping. *Geomech. Tunn.* **2016**, *9*, 29–36. [CrossRef]
9. Frodella, W.; Gigli, G.; Morelli, S.; Lombardi, L.; Casagli, N. Landslide mapping and characterization through infrared thermography (IRT): Suggestions for a methodological approach from some case studies. *Remote Sens.* **2017**, *9*, 1281. [CrossRef]
10. Mineo, S.; Calcaterra, D.; Perriello Zampelli, S.; Pappalardo, G. Application of Infrared Thermography for the survey of intensely jointed rock slopes. *Rend. Online Soc. Geol. It.* **2015**, *35*, 212–215. [CrossRef]
11. Pappalardo, G. First results of infrared thermography applied to the evaluation of hydraulic conductivity in rock masses. *Hydrogeol. J.* **2018**, *26*, 417–428. [CrossRef]
12. Pappalardo, G.; Mineo, S.; Imposa, S.; Grassi, S.; Leotta, A.; La Rosa, F.; Salerno, D. A quick combined approach for the characterization of a cliff during a post-rockfall emergency. *Landslides* **2020**, *17*, 1063–1081. [CrossRef]
13. Pappalardo, G.; Mineo, S.; Carbone, S.; Monaco, C.; Catalano, D.; Signorello, G. Preliminary recognition of geohazards at the natural reserve "Lachea Islet and Cyclop Rocks" (Southern Italy). *Sustainability* **2021**, *13*, 1082. [CrossRef]

14. Wu, J.H.; Lin, H.M.; Lee, D.H.; Fang, S.C. Integrity assessment of rock mass behind the shotcreted slope using thermography. *Eng. Geol.* **2006**, *80*, 164–173. [CrossRef]
15. Mineo, S.; Pappalardo, G. InfraRed Thermography presented as an innovative and non-destructive solution to quantify rock porosity in laboratory. *Int. J. Rock Mech. Min. Sci.* **2019**, *115*, 99–110. [CrossRef]
16. Huang, J.; Liu, S.; Gao, X.; Yang, Z.; Ni, Q.; Wu, L. Experimental Study of the Thermal Infrared Emissivity Variation of Loaded Rock and Its Significance. *Remote Sens.* **2018**, *10*, 818. [CrossRef]
17. Danov, M.; Stoyanov, D.; Tsanev, V. Measuring the spectral emissivity of rocks and the minerals that form them. *SPIE—Int. Soc. Opt. Eng.* **2007**. [CrossRef]
18. Baldridge, A.M.; Hook, S.J.; Grove, C.I.; Rivera, G. The ASTER Spectral Library Version 2.0. *Remote Sens. Environ.* **2009**, *113*, 711–715. [CrossRef]
19. Meerdink, S.K.; Hook, S.J.; Roberts, D.A.; Abbott, E.A. The ECOSTRESS spectral library version 1.0. *Remote Sens. Environ.* **2019**, *230*, 1–8. [CrossRef]
20. FLIR. User's Manual FLIR T6xx Series. 2017. Available online: https://www.flir.com/globalassets/imported-assets/document/flir-t6xx-series-user-manual.pdf (accessed on 21 April 2021).
21. Ciocia, C.; Marinetti, S. In-situ emissivity measurement of construction materials. In Proceedings of the 11th International Conference on Quantitative InfraRed Thermography, Naples, Italy, 11–14 June 2012.
22. Rivard, B.; Thomas, P.J.; Giroux, J. Precise Emissivity of Rock Samples. *Remote Sens. Environ.* **1995**, *54*, 152–160. [CrossRef]
23. National Aeronautics and Space Administration NASA, Science Mission Directorate. Infrared Waves. Retrieved from NASA Science Website. 2021. Available online: http://science.nasa.gov/ems/07_infraredwaves (accessed on 21 April 2021).
24. Havens, K.J.; Sharp, E.J. *Thermal Imaging Techniques to Survey and Monitor Animals in the Wild*; Academic Press: Cambridge, MA, USA, 2016. [CrossRef]
25. Hillel, D. *Environmental Soil Physics*; Academic Press: New York, NY, USA, 1998; p. 771.
26. Rinker, J.N. Airborne infrared thermal detection of caves and crevasses. *Photogramm. Eng. Remote Sens.* **1975**, *41*, 1391–1400.
27. Squarzoni, C.; Galgaro, A.; Teza, G.; Acosta, C.A.T.; Pernito, M.A.; Bucceri, N. Terrestrial laser scanner and infrared thermography in rock fall prone slope analysis. *Geophys. Res. Abstr.* **2008**, *10*, EGU2008-A-09254. Available online: https://meetings.copernicus.org/www.cosis.net/abstracts/EGU2008/09254/EGU2008-A-09254.pdf (accessed on 21 April 2021).
28. Baroň, I.; Bečkovský, D.; Míča, L. Application of infrared thermography for mapping open fractures in deepseated rockslides and unstable cliffs. *Landslides* **2014**, *11*, 15–27. [CrossRef]
29. Pappalardo, G.; Mineo, S.; Perriello Zampelli, S.; Cubito, A.; Calcaterra, D. InfraRed Thermography proposed for the estimation of the Cooling Rate Index in the remote survey of rock masses. *Int. J. Rock Mech. Min. Sci.* **2016**, *83*, 182–196. [CrossRef]
30. Pappalardo, G.; Mineo, S.; Calcaterra, D. Geomechanical Analysis of Unstable RockWedges by Means of Geostructural and Infrared Thermography Surveys. *Ital. J. Eng. Geol. Environ.* **2017**, 93–101. [CrossRef]
31. Fiorucci, M.; Marmoni, G.M.; Martino, S.; Mazzanti, P. Thermal Response of Jointed Rock Masses Inferred from Infrared Thermographic Surveying (Acuto Test-Site, Italy). *Sensors* **2018**, *18*, 2221. [CrossRef]
32. Casagli, N.; Frodella, W.; Morelli, S.; Tofani, V.; Ciampalini, A.; Intrieri, E.; Raspini, F.; Rossi, G.; Tanteri, L.; Lu, P. Spaceborne, UAV and ground-based remote sensing techniques for landslide mapping, monitoring and early warning. *Geoenviron. Disasters* **2017**, *4*, 9. [CrossRef]
33. Pappalardo, G.; Mineo, S.; Angrisani, A.C.; Di Martire, D.; Calcaterra, D. Combining field data with infrared thermography and DInSAR surveys to evaluate the activity of landslides: The case study of Randazzo Landslide (NE Sicily). *Landslides* **2018**, *15*, 2173–2193. [CrossRef]
34. Teza, G.; Marcato, G.; Pasuto, A.; Galgaro, A. Integration of laser scanning and thermal imaging in monitoring optimization and assessment of rockfall hazard: A case history in the Carnic Alps (Northeastern Italy). *Nat. Hazards* **2015**, *76*, 1535–1549. [CrossRef]
35. Guerin, A.; Jaboyedoff, M.; Collins, B.D.; Derron, M.-H.; Stock, G.M.; Matasci, B.; Boesiger, M.; Lefeuvre, C.; Podladchikov, Y.Y. Detection of rock bridges by infrared thermal imaging and modeling. *Sci. Rep.* **2019**, *9*, 13138. [CrossRef]
36. Luong, M.P. Infrared thermovision of damage processes in concrete and rock. *Eng. Fract Mech.* **1990**, *35*, 291–310. [CrossRef]
37. He, M.C.; Gong, W.L.; Zhai, H.M.; Zhang, H.P. Physical modeling of deep ground excavation in geologically horizontal strata based on infrared thermography. *Tunn. Undergr. Space Technol.* **2010**, *25*, 366–376. [CrossRef]
38. Junique, T.; Vazquez, P.; Thomachot-Schneider, C.; Hassoun, I.; Jean-Baptiste, M.; Géraud, Y. The Use of Infrared Thermography on the Measurement of Microstructural Changes of Reservoir Rocks Induced by Temperature. *Appl. Sci.* **2021**, *11*, 559. [CrossRef]
39. Mineo, S.; Pappalardo, G. Preliminary results on the estimation of porosity in intact rock through InfraRed Thermography. *Rend. Online Soc. Geol. It.* **2016**, *41*, 317–320. [CrossRef]
40. Mineo, S.; Pappalardo, G.; Casciano, C.I.; Di Stefano, A.; Catalano, S.; Gagliano, M. Insights on the Capo d'Orlando flysch (NE Sicily) by means of geomechanics and sedimentology. *Ital. J. Geosci.* **2019**, *138*, 404–417. [CrossRef]
41. Pappalardo, G.; Mineo, S.; Marchese, G. Effects of cubical specimen sizing on uniaxial compressive strength of Etna volcanic rocks (Italy). *Ital. J. Eng. Geol. Environ.* **2013**, *2*, 5–14. [CrossRef]
42. ASTM Designation: E 1933–99a. *Standard Test Methods for Measuring and Compensating for Emissivity Using Infrared Imaging Radiometers*; ASTM International: West Conshohocken, PA, USA, 2019.
43. Barreira, E.; Almeida, R.M.S.F.; Simões, M.L. Emissivity of Building Materials for Infrared Measurements. *Sensors* **2021**, *21*, 1961. [CrossRef] [PubMed]

44. Mashkov, P.; Pencheva, T.; Gyoch, B. Reflow soldering processes development using infrared thermography. In Proceedings of the 32nd International Spring Seminar on Electronics Technology, Brno, Czech Republic, 13–17 May 2009; pp. 1–6. [CrossRef]
45. Pappalardo, G.; Mineo, S. Investigation on the mechanical attitude of basaltic rocks from Mount Etna through InfraRed Thermography and laboratory tests. *Constr. Build. Mater.* **2017**, *134*, 228–235. [CrossRef]